Published online 30 December 2022

Nucleic Acids Research, 2023, Vol. 51, No. 1 ***41–53***
https://doi.org/10.1093/nar/gkac1214

DNA–protein cross-links between abasic DNA damage and mitochondrial transcription factor A (TFAM)

Wenyan Xu [1], Jin Tang[1] and Linlin Zhao [1,2,*]

[1]Department of Chemistry, University of California, Riverside, Riverside, CA 92521, USA and [2]Environmental Toxicology Graduate Program, University of California, Riverside, Riverside, CA 92521, USA

Received June 03, 2022; Revised November 25, 2022; Editorial Decision December 05, 2022; Accepted December 07, 2022

ABSTRACT

In higher eukaryotic cells, mitochondria are essential organelles for energy production, metabolism, and signaling. Mitochondrial DNA (mtDNA) encodes 13 protein subunits for oxidative phosphorylation and a set of tRNAs and rRNAs. mtDNA damage, sourced from endogenous chemicals and environmental factors, contributes to mitochondrial genomic instability, which has been associated with various mitochondrial diseases. DNA–protein cross-links (DPCs) are deleterious DNA lesions that threaten genomic integrity. Although much has been learned about the formation and repair of DPCs in the nucleus, little is known about DPCs in mitochondria. Here, we present *in vitro* and *in cellulo* data to demonstrate the formation of DPCs between a prevalent abasic (AP) DNA lesion and a DNA-packaging protein, mitochondrial transcription factor A (TFAM). TFAM cleaves AP-DNA and forms DPCs and single-strand breaks (SSB). Lys residues of TFAM are critical for the formation of TFAM-DPC and a reactive 3′-phospho-α,β-unsaturated aldehyde (3′pUA) residue on SSB. The 3′pUA residue reacts with two Cys of TFAM and contributes to the stable TFAM-DPC formation. Glutathione reacts with 3′pUA and competes with TFAM-DPC formation, corroborating our cellular experiments showing the accumulation of TFAM-DPCs under limiting glutathione. Our data point to the involvement of TFAM in AP-DNA turnover and fill a knowledge gap regarding the protein factors in processing damaged mtDNA.

INTRODUCTION

In the nucleus, DNA–protein cross-links (DPCs) are highly toxic DNA lesions that can interfere with almost all chromatin-based processes (1,2). DPCs form as intermediates in DNA repair or the topological transformations of DNA, or when cells are exposed to endogenous and exogenous chemicals, such as bifunctional electrophiles and chemotherapeutic agents (2,3). In addition, reactive DNA lesions, such as 5-formylcytosine and abasic (AP) sites, can lead to DPCs (2,4). Collectively, DPCs represent a broad spectrum of bulky DNA modifications with different cross-linking chemistry, flanking DNA structures, and protein sizes. Different types of DPCs known to date have been summarized in recent reviews (2,4).

Considering the abundance of AP sites (estimated at a steady-state level of 20 000–50 000 per cell) (5,6), AP-derived DPCs are considered a major source of endogenous DPCs (7–9). Historically, transient DPCs have been shown with a number of DNA repair enzymes with DNA glycosylase or AP-lyase activities (2,4). The formation of these enzymatic DPCs is primarily mediated by nucleophilic Lys residues and aldehydic lesions, such as AP sites, forming reversible Schiff base cross-links, which can be trapped in the presence of borohydride. In addition, a body of work by Greenberg and others has demonstrated the formation of histone DPCs with various forms of AP sites or other aldehydic lesions (7,10,11). Further, the recent discovery of SOS response-associated peptidase (SRAP)-domain proteins corroborate the importance of AP-derived DPCs. These proteins are conserved across all domains of life, with two prominent examples being the *Escherichia coli* AP-site processing protein YedK (12) and the human HMCES (5-hydroxymethylcytosine (5hmC) binding, embryonic stem cell-specific) protein (13,14). HMCES forms stable DPCs with AP sites to prevent error-prone repair pathways (13,14), or function as a repair intermediate (15). In general, the repair of DPCs requires a combined action of proteolytic enzymes to degrade the cross-linked protein and canonical DNA repair pathways (2,4).

Despite the accumulating knowledge regarding DPCs with nuclear DNA (nDNA), very little is known regarding the formation of DPCs in mitochondria. The multicopy mitochondrial DNA (mtDNA) genome encodes 37 genes essential for mitochondrial and cellular functions (16). mtDNA instability has been implicated in a plethora of human disorders and aging (16–21). Here, we demonstrate the formation of mitochondrial DPCs between AP sites and an abundant mtDNA-packaging protein,

*To whom correspondence should be addressed. Tel: +1 951 827 9081; Email: linlin.zhao@ucr.edu

mitochondrial transcription factor A (TFAM), *in vitro* and in HeLa cells. TFAM is considered a histone-like protein due to its role in coating and compacting mtDNA (22). Our biochemical data show that TFAM cleaves AP site-containing DNA (AP-DNA) and facilitates the formation of DPCs and DNA single-strand breaks (SSB). Several types of cross-linking chemistry were observed, including Schiff base and thia-Michael-type reactions. The resulting TFAM-DPCs are relatively stable and can be isolated from HeLa cells and detected using an enzyme-linked immunosorbent assay (ELISA). Importantly, glutathione (GSH) competes with TFAM for the formation of DPCs, as evidenced by the accumulation of TFAM-DPCs under limiting glutathione and induced mitochondrial AP sites in HeLa cells. These data argue for the involvement of TFAM in AP-DNA turnover and hint at a signaling role of DPCs and SSB in mtDNA degradation or purifying selection.

MATERIALS AND METHODS

Reactions of TFAM with AP-DNA

Recombinant human TFAM and AP-DNA were prepared as described previously (23). Reactions of AP-DNA with TFAM were carried out in the presence of 4 μM AP-DNA, 8 μM TFAM, 20 mM HEPES (pH 7.4), 90 mM NaCl, 20 mM EDTA, without or with 25 mM $NaBH_3CN$. Reaction products were quenched with 0.1 M $NaBH_4$ and digested by trypsin, followed by denaturing PAGE analysis. Proteolytic digestion with trypsin was performed using 60 μg of trypsin (Worthington) per 24 pmol of TFAM at 37°C for 2 h. Trypsin digestion was performed with all TFAM-DPC samples to facilitate migration into gels except when assigning different DPC species, whereby trypsin digestion was followed by proteinase K treatment. The digestion with proteinase K was used to convert peptides in peptide-DNA cross-links from trypsin cleavage to smaller peptide fragments. Digestion was performed with 1 unit of proteinase K (NEB, P8107S) per 24 pmol of trypsin-digested TFAM sample for 2 h at 37°C. To examine the thermostability of DPC, products from 1-h and 6-h reactions were heated at 90°C for 10 min before quenching with $NaBH_4$.

Thermostability of DPC

The stability of DPC under different temperatures was examined by incubating DPC resulting from a 24-h reaction with TFAM in the presence of 20 mM HEPES (pH 7.4), 90 mM NaCl, and 20 mM EDTA (same condition as the TFAM and AP-DNA reactions). The reaction mixture was heated in a dry bath incubator for 1 h under varying temperatures before quenching with 0.1 M $NaBH_4$. Control reactions were quenched with $NaBH_4$ before heating. The resulting products were quantified without trypsin digestion using a 7.5 × 10 cm SDS (0.1%)–urea (7 M)-PAGE (12%, 19:1) gel to obtain the relative abundance of the products.

Electrophoretic mobility shift assays (EMSA)

EMSA was used to determine the binding stoichiometry between TFAM and DNA following the reported procedures (23).

Terminal structures of SSB

The mild NaOH digestion was performed by incubating 4 μM AP-DNA at 37°C for 1 h in the presence of 0.3 M NaOH. The harsh NaOH digestion was performed by incubating 4 μM AP-DNA at 65°C for 1 h in the presence of 0.3 M NaOH. Reactions of AP-DNA with TFAM were carried out as described as above. The control reaction was performed by incubating 4 μM AP-DNA with 5 mM βMe under the same buffer conditions. Endo III digestion was with 4 μM AP-DNA at 65°C for 1 h in the presence of 30 units of *Thermotoga maritima* (*Tma*) endo III (NEB, M0291S), 10 mM HEPES pH 7.4, 10 mM $MgCl_2$. The post-reaction digestion by *E. coli* endo IV with either TFAM reaction or Endo III reaction was performed by incubating the reaction mixture with 10 units endo IV (NEB, M0304S) and 1 mM DTT at 37°C for 1 h. Reactions of AP-DNA with endo IV were with 4 μM AP-DNA, 10 units endo IV, 50 mM HEPES pH 7.4, 10 mM $MgCl_2$, and 1 mM DTT at 37°C for 1 h. Trapping of 3'-pUA in situ was achieved with 5 mM βMe included in the reaction. For derivatization with βMe, 5 mM βMe was added to the reaction mixture after reactions with TFAM or endo III. All samples were quenched with $NaBH_4$ before electrophoretic analysis on a 38 cm × 30 cm urea–TBE–PAGE (18%, 19:1) gel.

Analysis of DPC by mass spectrometry

TFAM-DPCs were prepared by reactions with AP(5′) (or AP_R(5′)) and TFAM under the same condition as described above for 24 h at 37°C. Reactions were quenched by 0.1 M $NaBH_4$ followed by incubation on ice for 30 min. The reaction products were digested by trypsin in 100 mM Tris–HCl pH 8.0 and 20 mM $CaCl_2$ at 37°C overnight. The digestion of DPC was monitored by an 8 × 10 cm SDS–urea (7 M)–PAGE (12%) gel. The resulting DNA-peptide cross-links were filtered through a 3 kDa molecular weight cut-off filter (Millipore) to enrich the DNA-peptide cross-links and to replace the reaction buffer with ammonium acetate buffer (10 mM ammonium acetate pH 5.5). DNA–peptide cross-links were concentrated to approximately 17 μl by a vacuum concentrator, followed by the addition of 1 μl nucleoside digestion mix (New England Biolabs, M0649S) and 2 μl 10× nucleoside digestion mix reaction buffer. The mixture was incubated at 37°C overnight to convert DNA-peptide cross-links to nucleoside-peptide cross-links. The sample was analyzed by LC–MS/MS, as described previously (24). The data analysis was performed with AP_CrosslinkFinder, followed by manual verification of cross-linked residues and annotation of the MS/MS spectra. The semi-quantification of cross-linked peptides was based on the integrated peak area in MS spectra.

Human cell cultures

Tet-on HeLa cells (Takara, 631183) were transduced with a lentiviral vector encoding tetracycline-inducible mitochondrially targeted human UNG1-Y147A (Addgene plasmid 46883). Before treatment with doxycycline, the cells were maintained in DMEM containing 4.5 g/l glucose (Life Technologies, 12100046), 10% (v/v) tetracycline-free FBS (Takara, 631106), 2 μg/ml of puromycin, and 100 mg/l

G418 at 37°C and 5% CO_2. When the confluence reached 60%, cells were treated with 1 mM BSO (final concentration) for 48 h followed by incubation with 2 μg/ml doxycycline for another 24 h to induce the expression of UNG1-Y147A. Untreated cells were cultured under the same condition with no doxycycline in the media. Cells were harvested through Trypsin/EDTA treatment and washed with 1×DPBS (Gibco, 14190) once before the flash freezing in liquid nitrogen and stored at -80°C until further analysis.

Isolation of mitochondria from HeLa cells

Mitochondria were extracted from cells using homemade buffers and components from an mtDNA isolation kit (Bio-Vision, K280). Briefly, 2.5×10^7 cells were resuspended in 5 mL of 1× cytosol extraction buffer, and the suspension was incubated on ice for 10 min. Cells were homogenized using an ice-cold Dounce tissue grinder with 80 passes. The homogenate was centrifuged at 1200 g for 5 min at 4°C. The supernatant was transferred to a new centrifuge tube and spun at 1200 g for another 4 min at 4°C. The supernatant was centrifuged at 15 000 g for 10 min at 4°C. To remove nDNA contaminants, the mitochondria pellet was treated with 200 U of turbo nuclease (Millipore Sigma, T4330) in 200 μl of reaction containing 5 mM HEPES buffer pH 7.4, 210 mM mannitol, 70 mM sucrose, 10 mM $MgCl_2$, 5 mM $CaCl_2$, 0.2% (w/v) BSA, 1× proteinase inhibitor cocktails (Thermo Fisher Scientific, A32955) for 15 min at 37°C. The suspension was supplemented by 1 ml of fresh 1× cytosol extraction buffer followed by centrifugation at 15 000 g for 10 min at 4°C. The pellet was washed with 1 ml of fresh 1×cytosol extraction buffer before further processing.

Western blotting

Cells or isolated mitochondria were resuspended in 50 μl of mitochondrial lysis buffer A (50 mM HEPES pH 7.4, 150 mM NaCl, 0.1% SDS, protease inhibitor cocktail), followed by incubation at 23°C for 10 min. The total protein concentration was determined by a BCA protein assay (Thermo Scientific, A53225). 15 μg of proteins were loaded onto a 4–20% Tris-glycine–SDS-PAGE gradient gel (7.5 cm × 10 cm). The resolved protein bands were transferred to a piece of 0.45 μm nitrocellulose membrane (Bio-Rad,1620115) at 80 V at 4°C for 1 h in 1× transmembrane buffer (25 mM Tris–HCl pH 8.2, 192 mM glycine and 30% (v/v) methanol). The membrane was blocked using a 3% BSA solution for 1 h at 23°C followed by incubation with 1/1000 diluted primary mouse anti-myc IgG antibody (GenScript, A00704-100) for myc-tagged UNG1, primary mouse anti-Flag IgG antibody (ThermoFIsher Scientific, 14-6681-82) for Flag-tagged TFAM, rabbit anti-TFAM IgG (Cell Signaling Technology, 7495S) for TFAM, and rabbit anti-TOM20 IgG (Cell Signaling Technology, 42406S) for Tom20 overnight at 4°C. After washing with 5 mL of 1×TBST (20 mM Tris pH 7.4 at 23°C, 150 mM NaCl, 0.1 % (w/v) tween-20) thrice, the membrane was incubated in 1/5000 diluted secondary HRP-conjugated anti-mouse IgG (R&D systems, HAF007) for 1 h at 23°C. The same dilution and incubation procedures were followed for fluorescent secondary IgG antibodies (i.e. Invitrogen, A-21422, goat anti-mouse antibody Alexa Fluor™ 555; Invitrogen, A-11034, goat anti-rabbit antibody Alexa Fluor™ 488). To image fluorescent antibodies, the membrane was scanned with a Typhoon imager after washing. For ECL substrates, after washing, the membrane was incubated in a solution containing ECL substrates (Thermo Scientific, 32209) and enhancers for 2 m at room temperature. The membrane was imaged on the ChemiDoc Touch Imaging System (Bio-Rad). The antibodies were stripped by incubation with a stripping buffer (Thermo Scientific, 46430) at room temperature for 15 min. Re-blocking was performed with 3% BSA at room temperature for 1 h before incubating with a different primary antibody. The secondary antibody applied for the rabbit primary antibody was the HRP conjugated goat anti-rabbit IgG (1/1000, Novus, NBP1-75297).

Quantification of AP sites

mtDNA was purified from isolated mitochondria from HeLa cells with a genomic DNA purification kit (NEB, T3010), eluted with a solution (40 μl) containing 10 mM HEPES pH 7.4 and 0.1 mM EDTA. The concentration of DNA was measured using a pico-green-based assay kit (Thermo Fisher Scientific, P7581). AP sites were measured using an AP-site counting kit (Dojindo, DK02-12) following the manufacturer's procedures. Briefly, 100 ng purified mtDNA was incubated in 70 μl of 10 mM ARP solution at 37°C for 1 h. The ARP-labeled DNA was purified through a ZYMO DNA clean and concentrator kit (ZYMO, D4014). The concentration of DNA was measured using a pico-green-based assay. The mtDNA sample was diluted to 0.5 ng/μl with a solution containing 10 mM HEPES pH 7.4 and 0.1 mM EDTA. Further, 60 μl of diluted DNA sample was mixed with 100 μl DNA coating solution (Thermo Scientific, 17250) and loaded into each well of a 96-well ELISA microplate (Greiner, 650061). The plate was incubated at room temperature overnight. The next day, the solution in the wells was discarded. Each well was washed with 250 μl of 1×TBST buffer 5 times. An HRP-streptavidin solution (1/4000 dilution) in 1×TBST buffer was added to the wells, and the microplate was incubated at 37°C for 1 h. After the wells were washed with 250 μl of 1×TBST buffer 5 times, 150 μl of the ELISA substrate (Abcam, ab171524) was added to the wells. The microplate was incubated at 37°C for 40 min. UV Absorbance at 650 nm was measured with a Synergy H1 plate reader. The absolute AP-sites/100 000 bp was calculated according to the AP-standard solution provided by the Dojindo kit (Dojindo, DK02).

Quantitative PCR

The genomic DNA was extracted and purified with a genomic DNA purification kit (NEB, T3010). The concentration of DNA was determined by a pico-green assay. 1 ng template DNA was applied for quantitative PCR targeting the $tRNA_{glu}$ gene for mtDNA and the b-globin gene for nDNA. The template was diluted 500-fold with 0.1% tween-20 for the amplification targeting $tRNA_{glu}$. The reaction was performed in a 10 μl solution containing 1×Phusion HF buffer, 200 μM deoxynucleoside triphosphate mixture, 10 μM mixed primers, and 0.2 units of Phusion polymerase

on a Bio-Rad CFX Connect Real-Time PCR Detection System (Bio-Rad, 1855201). The reactions were held at 98°C for 2 m, followed by a temperature program of 10 s at 98°C, 30 s at 65°C, and 30 s at 68°C for 45 cycles. The Ct-values were calculated by the CFX Maestro Software (Bio-Rad). The melting temperature was analyzed after the reaction to ensure specific products were amplified. The absolute copy number was calculated according to the standard curve of each specific target. The purity of mtDNA was calculated from the following equation:

$$Purity(\%) = \frac{CN_{mt} \times 16500 \times 500}{CN_{mt} \times 16500 \times 500 + CN_n \times 3.3 \times 10^9} \times 100\%$$

where CN_{mt} is for the absolute copy number of mitochondrial DNA, and CN_n is for the absolute copy number of nuclear DNA. The equation was based on the assumption that each set of human nuclear DNA is composed of 3.3 billion base pairs.

Quantification of DPC by ELISA

The development and validation our ELISA-based method for detecting TFAM-DPCs were described previously (25). Briefly, isolated mitochondria were resuspended in 50 μl of ice-cold 1× PBS, which contained 60 μg of RNase A (NEB, T3018L). 50 μl of cell-lysis buffer in the kit of NEB T3010 was added. The mixture was incubated on ice for 10 min followed by incubation with 0.1 M $NaBH_4$ for another 2 min. The sample was mixed with 700 μl of DNA binding solution in the ZYMO DNA clean and concentrator kit (ZYMO, D4014) and processed following the manufacturer's recommended procedure. The TFAM-mtDNA-crosslinks were eluted by incubating the column in 10 μl solution containing 20 mM HEPES pH 7.4, 0.1 mM EDTA and 0.1% SDS at room temperature for 10 min, followed by centrifugation at 13000 g and room temperature for 1 min. The flow through was loaded onto the column and processed through extraction again. The eluents were combined in one tube. The concentration of DNA was measured through a pico-green-based assay. DNA was diluted to 0.5 ng/μl with the 1×DNA coating solution (ThermoFisher, 17250). To each well of a tissue culture microplate (BRAND, 781965), 60 μl of the diluted DNA solution and 90 μl of DNA coating solution were added. The plate was incubated at room temperature overnight. The solution was aspirated, and the wells were washed with 1× TBST solution 5 times. The blocking was performed with 3% BSA in 1× TBST at room temperature for 1 h. The primary antibody, rabbit anti-human TFAM IgG (Cell Signaling, 7495S), was applied with 1/500 dilution followed by incubation at 4°C overnight. For Flag-tagged TFAM, primary mouse anti-Flag IgG antibody (ThermoFisher Scientific, 14-6681-82) was used with 1/500 dilution. After washing with 1× TBST, the wells were incubated in 1/1000 dilution of HRP conjugated goat anti-rabbit IgG (Invitrogen, A11034) at room temperature for 1 h. The luminescence was obtained from 150 μl of the substrate (Thermo, 37069) with a Synergy H1 plate reader. The change fold of the luminescence was normalized to the intensity from untreated cells.

Transient expression of wild-type TFAM and variants

Transient expression of wild-type TFAM with a C-terminal Flag tag was achieved by transfecting Tet-on HeLa cells with inducible UNG1-Y174A using a pCMV3-TFAM-FLAG vector. The vector contained TFAM cDNA ORF clone inserted between restriction sites KpnI and XbaI and was obtained from Sino Biological, Inc. (cat. No. HG15937-CF). The C49S/C246S (2CS) variant was prepared using a site-directed mutagenesis kit (New England Biolabs, E0554S) through sequential mutagenesis experiments (C49S followed by C246S). The primer sequences are shown in Supplementary Table S1. The plasmid was amplified using competent *E. coli* cells, and the sequence was confirmed by Sanger sequencing (Supplementary, Figure S10A). For transfection, Tet-on HeLa cells with inducible UNG1-Y147A were seeded into a 15-cm Petri dish. Once the confluence reached 60%, the media was replaced by fresh DMEM containing 4.5 g/l glucose. Two hours later, 1 μg of pCMV3-TFAM-FLAG vector containing wild-type TFAM or the 2CS variant was mixed with 50 μl of DharmaFECT kb DNA transfection reagent (Horizon Discovery, T-2006–01). The mixture was incubated at 23°C for 8 min and diluted with 150 μl of Opti-MEM (Gibco, 22600134). The diluted mixture was added to the culture drop by drop. After 2 hours, BSO was added into the culture to a final concentration of 1 mM. After a 48-hour incubation, doxycycline was added to a final concentration at 2 μg/ml, and cells was cultured for another 24 h to induce the expression of UNG1-Y147A.

Quantification of cellular glutathione

The total cellular glutathione (GSH and GSSG) was measured with a fluorometric assay kit (BioVision, K264-100) following the manufacturer's instructions. Briefly, 6×10^6 cells were resuspended in 100 μl of ice-cold glutathione assay buffer. 60 μl of the homogenate was transferred to a prechilled tube containing perchloric acid (6 N) followed by mixing. The tube was incubated on ice for 5 m followed by centrifugation at 13 000 g for 2 m at 4°C. The supernatant was collected. To 40 μl of the supernatant, 20 μl of ice cold 6 N KOH was added, followed by incubation on ice for 5 min. The sample was centrifuged at 13 000 g for 2 m at 4°C. Into each well of a 96-well microplate (Greiner, 655900), 10 μl of the supernatant, 70 μl of assay buffer, and 10 μl of the reduction agent mix were added, followed by incubation at 23°C for 10 min. Afterward, 10 μl of the *o*-phthalaldehyde probe was added, followed by incubation at 23°C for 40 min. Fluorescence was measured using a Synergy H1 plate reader equipped with a filter with excitation and emission wavelengths at 340 and 420 nm, respectively. The number of moles of glutathione was calculated according to the glutathione standard provided by the kit and was normalized to by the number of cells.

Cell viability assay

Tet-on HeLa cells were seeded in the wells of a 96-well microplate at a confluence of 50%. The next day, BSO was added to the media at a final concentration of 1 mM. Cells

were incubated for 48 h followed by incubation for an additional 24 h after 2 μg/ml doxycycline was added. The viability was measured with a cell counting kit (Dojindo, CK04). Briefly, the media were replaced with 100 μl of fresh media. 10 μl of the CCK-8 solution was added per well. After a 2-h incubation, the absorbance at 450 nm was measured using a Synergy H1 plate reader. The viability was calculated through the following equation:

$$Viability = \frac{Abs_{treted} - Abs_{blank}}{Abs_{untreated} - Abs_{blank}} \times 100\%$$

Statistical analysis

In all graphs, each data point was from an independent experiment. The difference between the treated and untreated samples was analyzed using the one-way ANOVA test.

RESULTS

Formation of TFAM-DPCs in vitro

TFAM promotes DNA strand cleavage at AP sites via Schiff base chemistry (23). To assess the accumulation of DPCs, we designed DNA substrates with a site-specific AP lesion and a fluorescein (FAM) label (Figure 1A, DNA sequences are shown in Supplementary, Table S1). The 3′-labeled AP(3′) allows the detection of various forms of products collectively as SSB, and the 5′-labeled AP(5′) (or AP_R(5′)) reveals any accumulated DPCs (Figure 1B). AP(5′) and AP(3′) are identical in sequence and the location of AP modification. The light-strand promoter (LSP) sequence (AP(3′), AP(5′)) was used to probe the putative Lys residues responsible for cross-linking in the TFAM-DNA complex on the basis of the defined polarity when TFAM binds to the LSP sequence (26,27). A substrate (AP_R(5′)) with a random sequence was used to show the generality of reactions (Figure 1A). Two types of DPCs were expected, DPC_{in} and DPC_{cl}, corresponding to a TFAM molecule covalently linked to intact or cleaved DNA before and after β-elimination, respectively (Figure 1B). Reactions of TFAM with AP-DNA were carried out under a stoichiometry ratio of 2:1, whereby AP-DNA was saturated with the highest yield of 1TFAM:1DNA complexes formed (Supplementary, Figure S1). In situ trapping of Schiff base intermediates formed between an AP lesion and a Lys residue was achieved by carrying out reactions in the presence of $NaBH_3CN$. All reactions were quenched with $NaBH_4$ to prevent the spontaneous degradation of AP sites or imine intermediates during sample workup and gel electrophoresis.

TFAM-DPCs were converted to peptide-DNA cross-links via trypsin digestion to facilitate electrophoresis and quantitation. For simplicity, peptide-DNA cross-links will be referred to as DPCs without differentiating the two. In the presence of $NaBH_3CN$, Schiff base intermediates were trapped in the reduced form and refractory to β-elimination (DPC_{in}, Fig 1B), as evidenced by the co-migrating products from reactions with AP(5′) or AP(3′) and the lack of SSB in these reactions (Figure 1C, lanes 5–8). Treating trypsin-digested products with a nonspecific protease, proteinase K, converted the product band to a series of smaller products migrating slower than AP-DNA substrates (Figure 1D, compare lane 2 to 3 and lane 4 to 5), indicative of products containing a full-length DNA oligomer and peptide fragments of varying sizes. These observations confirm the major product band in Figure 1C lanes 5, 6 and 8 to be DPC_{in}. Without $NaBH_3CN$, the reaction could proceed to form the ultimate product, SSB (Figure 1C, lanes 1–4). Notably, besides SSB, three additional product bands were observed in reactions with AP(5′), (Figure 1C, lane 4), indicative of the presence of a 5′-labeled DNA fragment. As expected, these products were not observed in reactions with AP(3′), whereby all products were observed in the form of SSB (Figure 1C, lane 2). The accumulated products with AP(5′) were confirmed to be DPC on the basis of proteolytic digestion (Figure 1D, compare lane 6 to 7). Of the three DPC bands (Figure 1C, lane 4), the top band migrated faster than DPC_{in} and likely corresponded to a product with a partial DNA strand (DPC_{cl}). The assignment was verified by its conversion to products migrating faster than the substrate DNA upon proteinase K digestion (Figure 1D, compare lane 6 to 7). The other two product bands were assigned as DPC_{cl} due to their faster migration relative to AP(5′) (Figure 1C, lane 4) and their conversion into smaller products upon proteolytic digestion (Figure 1D, compare lane 6 to 7). Further, different forms of SSB were assigned by comparing with standards from mild alkaline treatment based on the known chemistry to form β and β,δ-elimination products (Figure 1C, lane 9 and *vide infra*). Together, these results demonstrate that in addition to SSB, TFAM-DPCs can accumulate when TFAM cleaves AP-DNA, even in the absence of chemical trapping.

Thermostability of TFAM-DPCs

Considering the importance of the Schiff base in TFAM-DPC formation and the heat lability of imine, we examined the thermostability of DPCs. Upon heating at 90°C, products from 1 and 6-h reactions with AP(5′) or AP(3′) in the absence of $NaBH_3CN$ were converted to the ultimate products, SSB (Figure 1C, lanes 11–14), in keeping with the heat lability of Schiff base. To evaluate their thermostability under different temperatures, we prepared DPCs using TFAM and AP(5′). The reaction time was allowed for 24 h to ensure a near complete conversion of the substrate AP(5′) to DPCs so that the observed SSB was indeed released from DPCs rather than the spontaneous β-elimination of AP sites. Heating the resulting DPCs under increasing temperatures led to a gradual decrease in the amount of remaining DPCs (Figure 1E, top; Supplementary, Figure S2). Nonetheless, approximately 20% DPC remained after heating at 90°C for 1 h. Similarly, approximately 20% of remaining DPCs were also observed with AP_R(5′) (Figure 1E; Supplementary, Figure S2), indicative of the presence of stable DPC with a random DNA substrate. These data demonstrate the formation of heat-stable DPCs between TFAM and AP-DNA, suggesting that additional cross-linking chemistry exists other than the Schiff base.

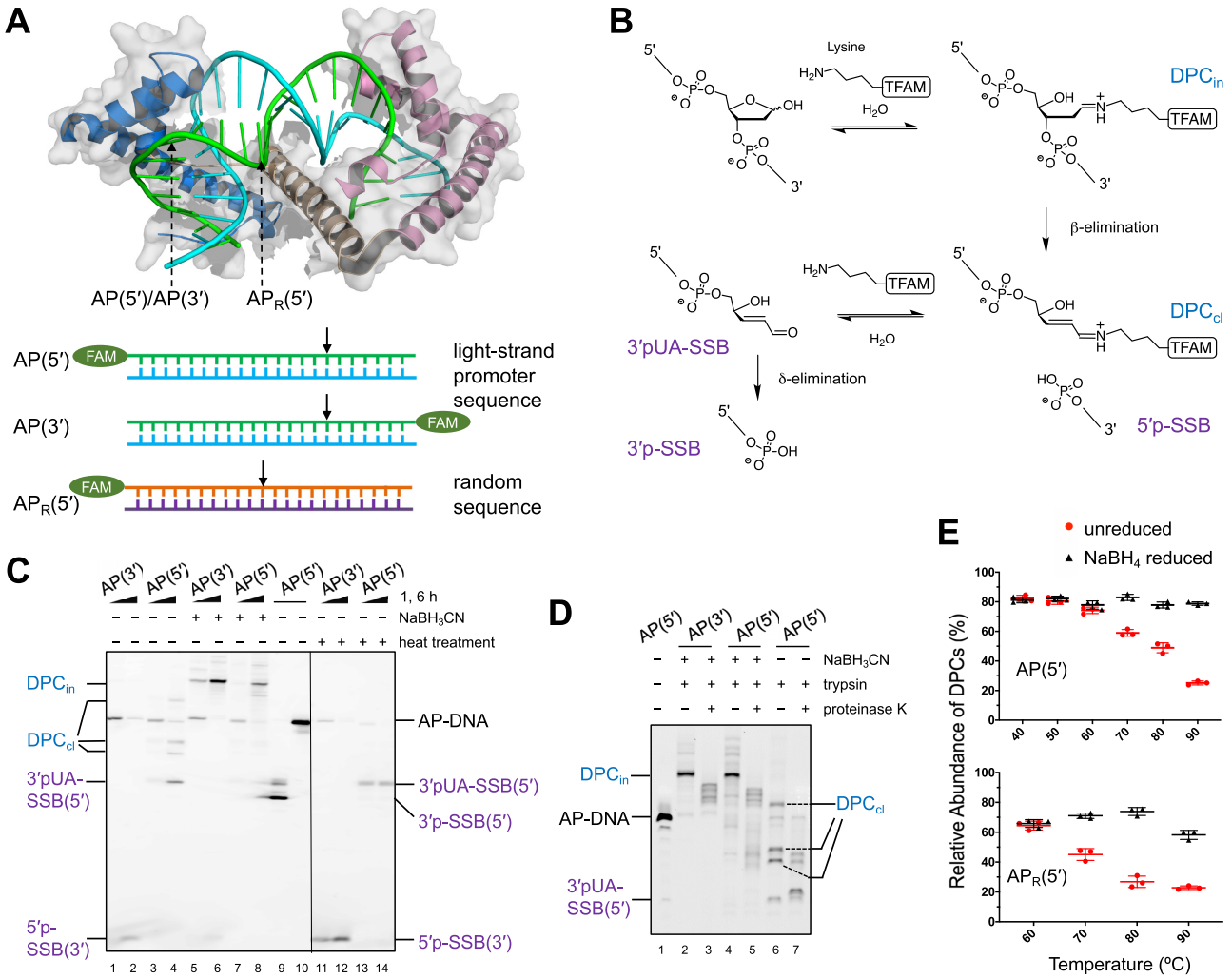

Figure 1. Formation of DPCs between TFAM and AP sites. (**A**) Crystal structure of TFAM-DNA complex with the mitochondrial light-strand promoter (LSP) sequence (PDB: 3TQ6). The two high-mobility group (HMG) box domains of TFAM are in pink (HMG1) and blue (HMG2), and the inter-domain linker is in wheat. The heavy strand is in cyan, and the light strand is in green. For different substrates, the positions of AP sites within the structure are indicated by arrows. The lower panel depicts three types of AP substrates. AP(5′) and AP(3′) are identical in sequence and the location of AP modification, and are in LSP sequence with a 5′ 6-fluorescein (FAM) and 3′ FAM, respectively. AP$_R$(5′) contains a random sequence. (**B**) Proposed reaction mechanism of TFAM-mediated AP-DNA cleavage. DPC$_{in}$, DPCs with full-length DNA; DPC$_{cl}$, DPCs with cleaved DNA; 3′pUA-SSB, SSB with a 3′-phospho-α,β-unsaturated aldehyde residue. (**C**) Denaturing PAGE analysis of reactions of TFAM with AP(3′) or AP(5′) for 1 and 6 h. Products were digested with trypsin to facilitate their migration into gels. Lanes 1–4 are reactions without NaBH$_3$CN trapping; Lanes 5–8 are reactions with NaBH$_3$CN trapping; lane 9, SSB standards after β and β,δ-elimination reactions under alkaline cleavage (0.3 M NaOH, 37°C, 1 h); lane 10, AP-DNA standard after NaBH$_4$ reduction. DPC$_{in}$ was assigned by comparing products from AP(3′) and AP(5′) under NaBH$_3$CN reduction (lanes 6 and 8). Most DPC products were heat-labile and converted to SSB after heating at 90°C for 10 min (lanes 11–14). (**D**) Proteolytic digestion of DPC from a 6-h reaction facilitated the assignment of DPC$_{in}$ and DPC$_{cl}$. (**E**) Thermostability of DPCs treated for 1 h under different temperatures. DPCs were from reactions with TFAM and AP(5′) or AP$_R$(5′) for 24 h at 37°C without NaBH$_3$CN. Products quenched with NaBH$_4$ are labeled as black triangles; products treated by heating before quenching with NaBH$_4$ are labeled as red spheres. Data are average values with S.D. ($n = 3$). The amount of DPCs is shown as the relative abundance of all products (DPC and SSB).

Chemistry of TFAM-DPCs

To decipher the chemistry of DPCs, we characterized the terminal structures of SSB from TFAM-catalyzed reactions. We verified the formation of a reactive 3′-phospho-α,β-unsaturated aldehyde residue (3′pUA, shown in Figure 2A) by comparing products with those from well-characterized reactions from NaOH or DNA glycosylase-catalyzed reactions (28), or by trapping with thiol-containing chemicals, such as β-mercaptoethanol (βMe) or GSH. Small molecule thiols (29,30) or Cys residues (31) are known to be able to conjugate with an α,β-unsaturated aldehyde via 1,4-addition. As shown in Figure 2B (lanes 2, 3, 14, and 15), reactions with AP(5′) under mild and strong NaOH treatment proceeded primarily via β-elimination and β,δ-elimination, respectively. TFAM-mediated AP-DNA cleavage produced two SSB products corresponding to β-elimination and β,δ-elimination products. Treating the TFAM-catalyzed products with *E. coli* endo IV led to the conversion of the bottom band to a slower migrating product (Figure 2B, lane 8), supporting the assignment of the bottom band as 3′p-SSB given

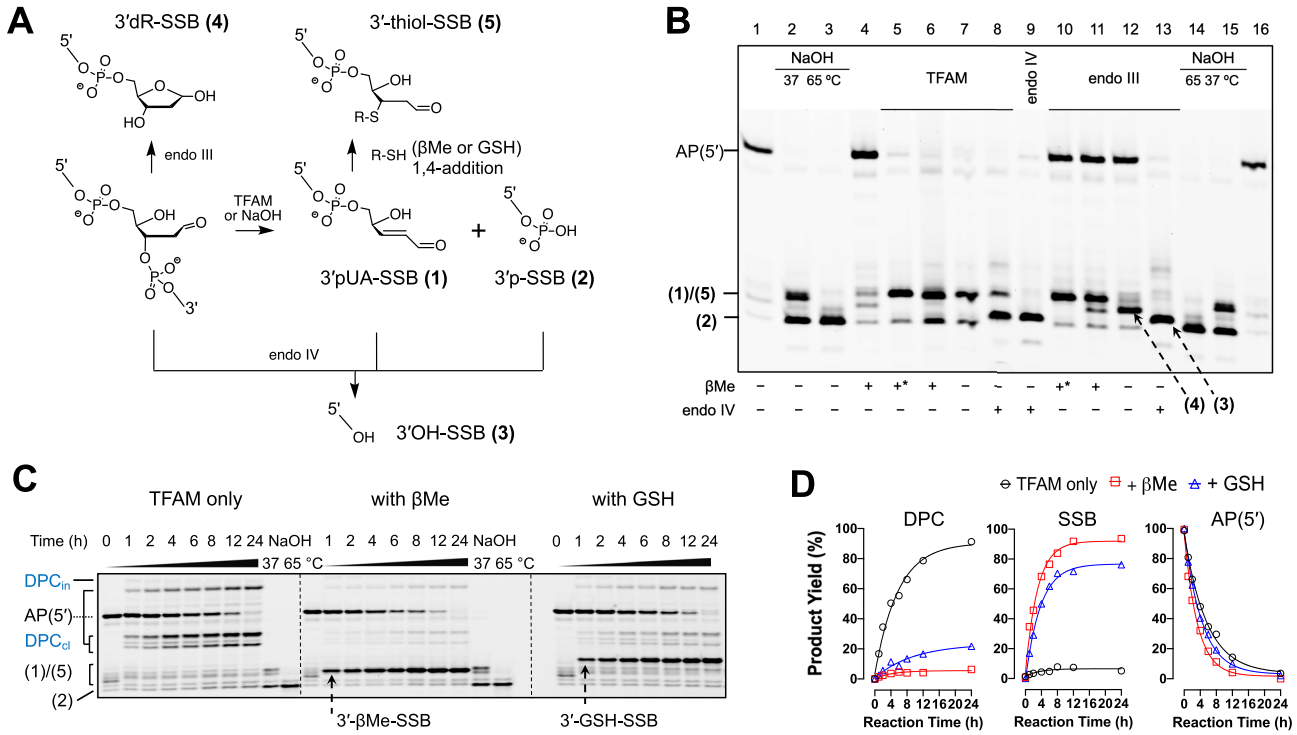

Figure 2. Elucidation of the terminal structures of SSB in TFAM-mediated reactions. (A) Proposed reaction mechanisms by which AP-DNA undergoes strand cleavage reactions catalyzed by TFAM, NaOH, endo III, or endo IV glycosylase. The resulting 3′ pUA-SSB can be trapped by thiol-containing chemicals, such as βMe or GSH. Product 1 is 3′pUA-SSB; 2 is 3′p-SSB, 3 is 3′OH-SSB; 4 is 3′dR-SSB; 5 is thiol-conjugates after reactions with βMe. (**B**) Gel electrophoretic analysis of reaction products of AP(5′) with NaOH, TFAM, endo III, or endo IV glycosylase. Reactions with asterisks indicate the presence of 5 mM βMe during the reaction for trapping 3′pUA *in situ*; reactions without asterisks indicate products were derivatized with βMe after TFAM-mediated reactions. All reactions were quenched with $NaBH_4$ before denaturing PAGE analysis. (**C**) Reaction time courses of AP(5′) with TFAM (left), in the presence of 10 mM βMe (middle), or 10 mM GSH (right). The resulting DPCs were converted to peptide-DNA cross-links via proteolytic digestion to facilitate their migration. (**D**) Quantification of formation of DPC and SSB and disappearance of AP(5′).

the 3′ diesterase activity of endo IV (32). The formation of 3′pUA in TFAM-mediated reactions was also evidenced by the derivatized products with βMe (3′-thiol-SSB) (Figure 2B, lanes 5 and 6) and mass spectrometric characterizations (*vide infra*). Although the difference in migration of 3′-βMe-SSB and 3′pUA-SSB was small, additional reactions with GSH led to a significant difference in the migration patterns of 3′-thiol-SSB (Figure 2C and *vide infra*). Importantly, incubating AP(5′) with βMe alone did not produce appreciable amounts of SSB (Figure 2B, lane 4), supporting the role of TFAM in catalyzing the formation of 3′pUA.

We compared the TFAM-derived products with those from reactions with AP(5′) and endo III. Although endo III is generally perceived to produce 3′pUA with AP sites, reports by Gates (28) and others (33,34) argue for the formation of a 3′-deoxyribose (3′dR) residue owing to the conjugate addition of water to 3′pUA. In our hands, reactions with endo III produced a major product migrating in between products 1 and 2 (Figure 2B, lane 12) along with minor smeared products migrating similarly to 3′pUA-SSB (Figure 2B, lane 2, top band). The main product likely corresponds to 3′dR-SSB formed via the addition of water to the 3′pUA moiety, consistent with previous reports (28,33,34). The addition of βMe at the end of the endo III reaction led to the conversion of a majority of the 3′dR-SSB to the thiol-conjugates (Figure 2B, compare lane 11 to 12) due to the stronger nucleophilicity of thiol relative to water. On the other hand, reactions of endo III in the presence of βMe trapped the formation of 3′pUA *in situ* by forming the thiol conjugates (Figure 2B, compare lane 10 to 12), reaffirming the formation of 3′pUA as an intermediate, but not necessarily as an ultimate product, in endo III-catalyzed reactions. The formation of 3′dR in the endo III reaction, but not in the TFAM reaction, indicates that a water molecule is likely to be activated by specific interactions at the endo III active site. Evidently, TFAM-catalyzed reactions produced 3′pUA-SSB and did not involve the conjugate addition of water. Similarly, in a reaction with a random substrate (AP_R(5′), TFAM also produced β-elimination and β,δ-elimination products, albeit at slightly different yields compared to AP(5′) (Supplementary, Figure S3), which likely arise of different local interactions with the two types of TFAM-DNA complexes. Collectively, the thermostability of DPCs and the formation of 3′pUA-SSB in TFAM-mediated AP-DNA cleavage imply the presence of multiple cross-linking types in TFAM-DPCs.

Considering that GSH is present at millimolar concentrations in mitochondria (35), we carried out reactions over a time course with TFAM and AP-DNA in the presence of GSH or βMe. As observed in Figure 2C (left and middle panels), reactions in the presence of βMe produced βMe-

conjugated SSB (3′-βMe-SSB) migrating slightly slower than SSB products formed in TFAM reactions. The 3′-βMe-SSB formed at the expense of TFAM-DPCs (Figure 2C, middle panel), likely due to a 1,4-addition reaction of βMe to 3′pUA-SSB formed as a result of TFAM Lys-mediated catalysis. Trapping 3′pUA-SSB with glutathione retarded their migration even further (3′-GSH-SSB, Figure 2C, right panel), supporting the slow-migrating species being thiol-conjugates (product 5, Figure 2A). Similarly, thiol conjugates formed at the expense of DPCs, as observed in Figures 2C and D, suggesting that GSH can suppress the DPC formation. The presence of thiol did not significantly alter the rate of AP-DNA cleavage by TFAM (Figure 2D and Supplementary, Table S2), indicating that the TFAM-mediated cleavage of AP sites is efficient. The effect of GSH was also confirmed with a random DNA substrate $AP_R(5')$ (Supplementary, Figure S4 and Table S2), confirming the generality of the reaction. Together, these data demonstrate that the formation of DPCs depends on the formation of 3′pUA-SSB and that 3′pUA-SSB reacts with GSH at the expense of TFAM-DPCs, suggesting a regulatory role of GSH for TFAM-DPCs.

Identification of cross-linked amino acid residues in TFAM-DPC

To pinpoint the amino acid residues of TFAM involved and to characterize the chemical structures, we analyzed the TFAM-DPC derived from AP(5′) or $AP_R(5')$ using tandem mass spectrometry. Two predominant types of peptides were observed, i.e. peptides cross-linked at a Lys residue in the presence of $NaBH_3CN$ and peptides cross-linked at a Cys residue in the absence of $NaBH_3CN$. We obtained the relative abundance of peptides based on semi-quantification by integrated peak areas in MS spectra. In the presence of $NaBH_3CN$, a mass adduct (431) accounted for >99% of the abundance of all observed peptides (Figures 3A and B, Supplementary, Figure S5, Tables S3 and S5). TFAM cross-linked with AP(5′) primarily at K186 (Figures 3B and E), consistent with K186 being the closest Lys residue to the AP lesion in TFAM-DNA crystal structures (26,27). These observations support the involvement of K186 in the reaction. Aside from K186, several additional Lys residues were captured, albeit at a much lower overall abundance (Figure 3E). These DPCs could stem from the alternative conformations or dynamics of TFAM-DNA complexes reported by us (24) and others (36). A control experiment with a different substrate $AP_{20}(5')$ (sequence shown in Table S1) harboring an AP lesion at a position 3-nt away (5′ of) from AP(5′) led to a significant decrease in the relative abundance of TFAM-DPCs at K186 (76% to 18%, Figure 3E and Supplementary, Figure S6A and Table S7). The observation confirms the importance of K186 in the AP lyase activity.

In the absence of $NaBH_3CN$, a mass adduct (118) accounted for > 99% of the abundance of all observed peptides with AP(5′) (Supplementary, Figure S5, Tables S4 and S6). C49 was the major residue conjugated to the reduced form of 3′-pUA by $NaBH_4$ (Figures 3C and D). The product can be attributed to a Michael-type reaction (1,4-addition) between the sulfhydryl group of C49 and 3′-pUA. In addition, C246 contributed to the cross-linking to a lesser extent. Such DPC products confirm the formation of 3′pUA and provide a plausible explanation for the heat-stable DPCs observed in thermostability experiments. With a random DNA substrate $AP_R(5')$, TFAM was also cross-linked with the AP lesion via K186 under $NaBH_3CN$ trapping, implying that K186 is a critical residue in these reactions. Alternatively, the observation can be attributed to the modulation of the TFAM-DNA conformation by $AP_R(5')$ (37). It is likely that the polarity of TFAM binding to $AP_R(5')$ resembles that in the LSP-DNA complex due to the presence of a cryptic G residue in the substrate sequence (38). In the absence of $NaBH_3CN$, TFAM linked with $AP_R(5')$ primarily via C49, with DPC via C246 being a minor product, indicative of the breadth of the observed reactions. Notably, when a similar experiment was performed with a TFAM variant (C49S) and AP(5′) in the absence of $NaBH_3CN$, C246 became the predominant residue in cross-linking with the AP modification, reaffirming the role of Cys in forming (meta)stable DPCs (Supplementary, Figure S6B and Table S8). When comparing the DPC yields using gel-based assays, we observed no difference in the overall DPC yields between wild-type TFAM and C49S, supporting that C246 complements C49 in the DPC formation (Supplementary, Figure S7). Together, these data demonstrate unambiguously that Lys residues catalyze the formation of DPC and SSB and that the resulting 3′pUA-SSB contributes to the accumulation of (meta)stable TFAM-DPCs via Cys residues.

Formation of TFAM-DPCs in HeLa cells

To validate the formation of TFAM-DPCs in cells, we used a lentiviral system to generate mitochondrial AP sites by expressing a human UNG1 variant (Y147A) targeting mitochondria (39). UNG1-Y147A cleaves thymine in addition to uracil in mtDNA to produce mitochondrial AP sites (40). Compared to treating cells with a DNA-damaging reagent, which often leads to both nDNA and mtDNA damage, mitochondrial specific DNA damage in the form of AP sites avoids complex cross-talk between nDNA and mtDNA damage response pathways (41,42). The expression of myc-tagged UNG1-Y147A was induced by doxycycline, as evidenced by western blotting (Figure 4A). UNG1-Y147A expression for 24 h led to a moderate increase of AP sites, as demonstrated by an aldehyde reaction probe (ARP)-based assay (Figure 4B, ND vs. NN). Induction of AP sites was accompanied by a dramatic decline in mtDNA copy number (Figure 4C), as reported previously (39), suggesting that a majority of UNG1-Y147A-induced AP sites were processed rapidly via mtDNA degradation. The decrease in mtDNA copy number correlates with a decline in the TFAM level (Figure 4A). Considering the importance of GSH in the DPC formation, we examined the formation of TFAM-DPCs under limiting GSH in HeLa cells. The cellular level of GSH was suppressed by a known inhibitor of γ-glutamylcysteine synthetase, L-buthionine-(S,R)-sulfoximine (BSO) (43). Experimental conditions (1 mM BSO for 48 h followed by an additional 24-h incubation with 2 μg/ml doxycycline) were chosen without affecting the cell viability (Supplementary, Figure S8). After incubation with BSO, the total cellular GSH (sum of GSH and GSSH) decreased by ∼30% (BN and BD in Figure 4D).

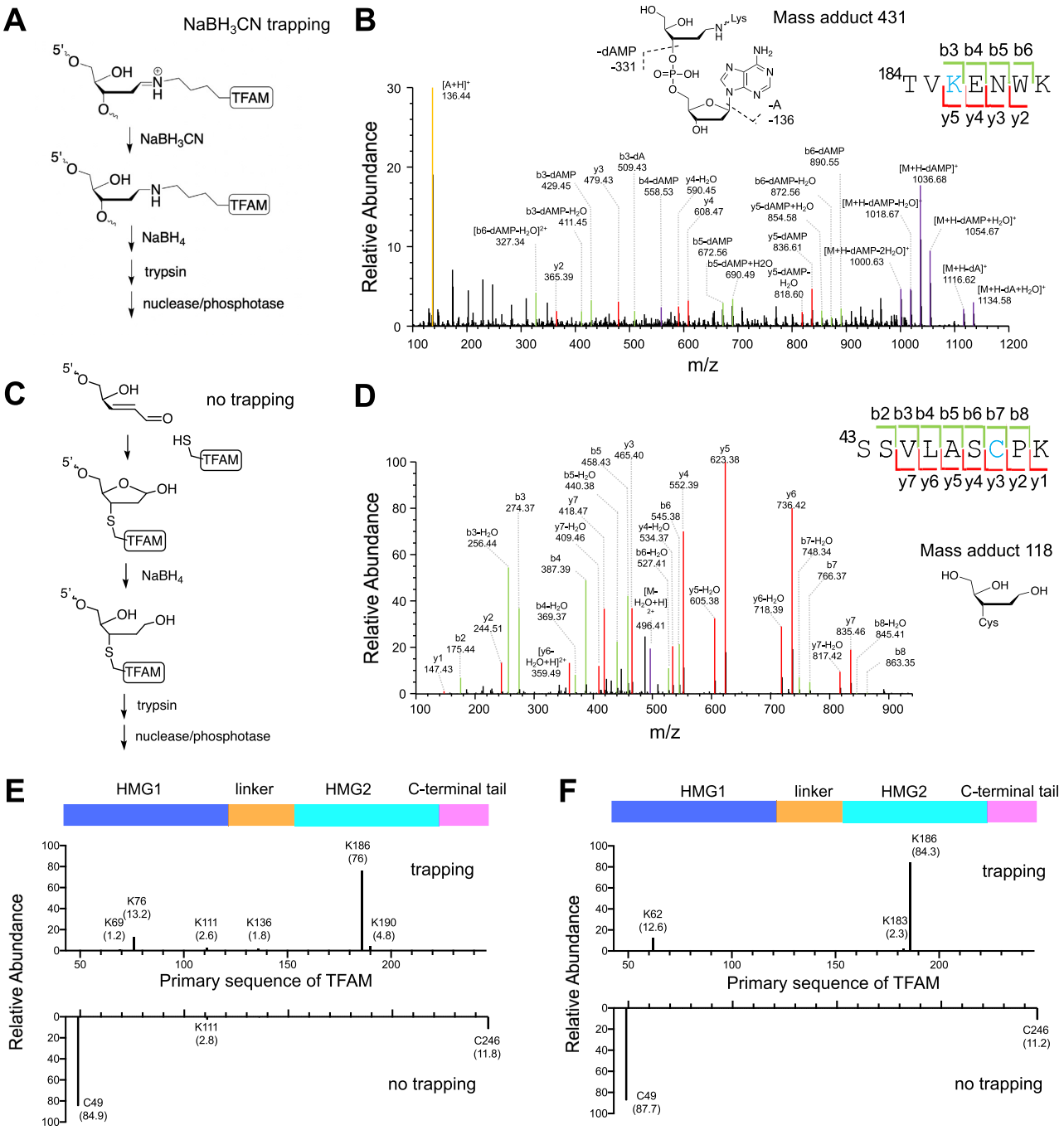

Figure 3. Identification of cross-linked amino acid residues in DPCs by mass spectrometry. (**A**) Sample preparation in the presence of $NaBH_3CN$ trapping to reduce the Schiff base intermediates. (**B**) Representative MS^2 spectrum of TFAM peptide fragmentation with K186 cross-linked via a reduced Schiff base with an AP residue (mass adduct 431). A neighboring nucleoside (dA) is present due to incomplete nucleoside digestion. (**C**) In the absence of $NaBH_3CN$ trapping, cysteine residues of TFAM reacted with 3′ pUA to form conjugates. (**D**) Fragmentation of TFAM peptide cross-linked at C49 with a reduced AP residue (mass adduct 118). (**E**) Relative abundance of observed cross-linked TFAM amino acid residues with AP(5′). Major residues were K186 in the presence of chemical trapping and C49 without trapping. A scheme of TFAM domains is shown on top. The numbers in parentheses indicate the relative abundance of DPCs calculated from integrated peak areas in MS spectra. (**F**) Relative abundance of observed cross-linked TFAM amino acid residues with $AP_R(5')$. Major residues were K186 in the presence of chemical trapping and C49 without trapping.

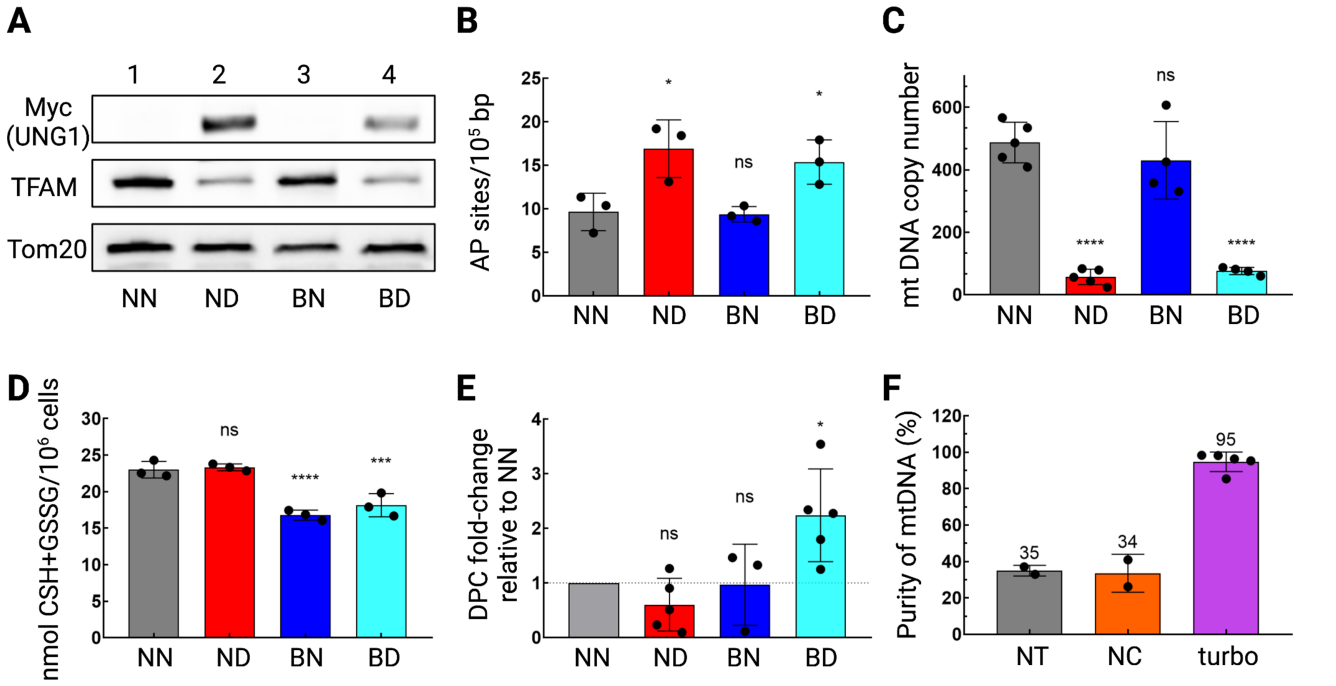

Figure 4. Formation of TFAM-DPCs in mitochondria of HeLa cells. (**A**) Confirmation of the expression of Myc-tagged UNG1-Y147A in mitochondria of HeLa cells by western blotting. Tom20 was used as a loading control. UNG1-Y147A contained a Myc tag. Treatment conditions were indicated by two-letter codes. The first letter indicates whether BSO is present, with N denoting untreated cells and B denoting BSO-treated cells. The second letter indicates whether the cells were treated with doxycycline, with D denoting doxycycline-induced expression of UNG1-Y147A and N denoting untreated cells. (**B**) Quantification of AP sites in mtDNA using ARP assays. (**C**) mtDNA copy-number by RT-PCR, normalized by the nDNA copy number based on the β-globin gene. (**D**) Quantification of total cellular glutathione. (**E**) The fold-change of TFAM-DPCs relative to untreated cells based on ELISA. (**F**) Purity of mtDNA in the assays. NT, nontreated mtDNA from isolated by differential centrifugation; NC, negative control, mock reactions without turbonuclease; turbo, turbonuclease treatment. Data were from independent experiments as indicated and were mean ± S.D. (or range of data for NN and NC in panel F). For NN in (E), the fold-change was normalized to control in each independent experiment, and therefore NN represents the mean from five independent experiments without showing the error bar. * indicates $P < 0.05$; *** indicates $P < 0.001$; **** indicates $P < 0.0001$; ns indicates no significant difference.

To quantify TFAM-DPCs in HeLa cells, we devised an ELISA-based method to measure TFAM-DPCs (25). ELISA was chosen to measure the total amount of TFAM covalently attached to mtDNA regardless of the cross-linking chemistry. To avoid interference from residual non-covalently associated TFAM during mtDNA isolation, we compared the fold change in ELISA signals relative to the control cells to determine whether there was an increase in the TFAM-DPC level. As shown in Figure 4E, the expression of UNG1-Y147A alone did not elevate the DPC level, presumably due to inhibition by GSH as observed in our biochemical assays. The comparable level of ELISA signals between NN and ND was not due to the lower amount of mtDNA as a result of mtDNA copy number decline because equal amounts of DNA from different samples were coated onto the ELISA plate. On the other hand, when GSH was suppressed, a moderate but statistically significant accumulation of TFAM-DPCs was observed, corroborating our biochemical experiments (Figure 2C). The moderate increase could arise from the rapid processing of these deleterious DNA lesions. Nonetheless, the statistically significant increase of DPCs implies that TFAM-DPCs were sufficiently stable within the cells and during mitochondrial isolation and purification, although 0.1 M $NaBH_4$ was added upon mitochondrial lysis to prevent spontaneous degradation of DPCs during sample workup. Presumably, the observed TFAM-DPC in ELISA may comprise a combination of DPCs involving Lys and Cys, on the basis of our mass spectrometry data. To avoid the potential bias sourced from nDNA in AP lesion quantification and DPC measurements, we eliminated the contaminating nDNA in the purified mtDNA samples by including a nuclease digestion step during mitochondria isolation. The purity of mtDNA samples for AP and DPC measurements was greater than 95%, as evidenced by qPCR results (Figure 4F; Supplementary, Figure S9).

Given the importance of two Cys residues in TFAM-DPC formation, we compared the TFAM-DPC levels in HeLa cells expressing ectopically the Flag-tagged wild-type TFAM or the Flag-tagged TFAM variant C49/C246(2CS). Ectopic expression was achieved by transfecting Tet-on HeLa cells (with inducible UNG1-Y147A) using a pCMV3-TFAM-FLAG vector. We verified that transient overexpression of Flag-tagged wild-type TFAM or 2CS did not alter mtDNA copy number under each condition (Supplementary, Figure S10D). The expression levels were comparable for Flag-tagged wild-type TFAM and 2CS. On the basis of the observed increase in TFAM-DPC levels in doxycycline and BSO-treated cells, we adapted the ELISA-based assays to detect Flag-tagged DPCs using an anti-Flag IgG antibody. ELISA signals were normalized to cells without doxycycline and BSO treatment. Our results show that the

expression of Flag-tagged wild-type TFAM led to a statistically significant increase in the Flag-TFAM-DPC level under doxycycline and BSO treatment (Supplementary, Figure S10E), similar to results with endogenous TFAM. On the other hand, the expression of the Flag-tagged C49/C246 TFAM variant showed no change in the Flag-TFAM-DPC level under doxycycline and BSO treatment (Supplementary, Figure S10E). The effect on DPC was not due to compromised expression of 2CS, because comparable levels of Flag-tagged TFAM were observed in the wtTFAM-Flag and C49S/C246S(2CS)-Flag-expressing cells (Supplementary, Figures S10B and S10C). These observations reaffirm the importance of Cys residues in the TFAM-DPC formation in living cells. Overall, these results from HeLa cells corroborate our biochemical data and argue for the involvement of TFAM in AP-site processing in human cells and a regulatory role of GSH for TFAM-DPC formation.

DISCUSSION

In response to mtDNA damage, mtDNA undergoes DNA repair, degradation, and compensatory DNA synthesis in the context of mitochondrial dynamics and mitophagy (16). In particular, mtDNA degradation has emerged as a crucial mechanism to counteract mtDNA damage regardless of lesion types (39,44). Nonetheless, it remains elusive regarding how mtDNA degradation occurs. In human cells and mice, several enzymes have been shown to participate in mtDNA degradation, i.e. mitochondrial genome maintenance exonuclease 1 (MGME1) (45), the exonuclease domain of DNA polymerase γ (46,47), and Flap endonuclease 1 (FEN1) (48). Given the abundance of TFAM in mitochondrial nucleoids, we explored the role of TFAM as a processing factor for ubiquitous AP sites. Our data demonstrate unequivocally that TFAM interacts with AP-DNA and produces DPCs *in vitro* and *in cellulo*. The reaction was facilitated by abundant Lys residues in TFAM (∼15% of the total number of amino acid residues) via Schiff base chemistry, as evidenced by mass spectrometry data in the presence of chemical trapping. The reaction produced highly reactive 3′pUA at the termini of SSB, which were susceptible to additional reactions with TFAM and GSH. Mass spectrometry and gel-based experiments demonstrate that TFAM C49 and C246 were complementary in cross-linking with 3′pUA-SSB, with C49 being the major residue. Our cellular experiments show that TFAM-DPCs were sufficiently long-lived in cells and can be isolated and detected under limiting GSH and induced mitochondrial AP sites. Notably, Yang and colleagues also showed that the half-life of Schiff base DPCs derived from histone and 3′-pUA ranges from 10 to 14 h in vitro (49). Overall, our observations of the important role of GSH in forming GSH-adducted SSB and in competing with TFAM in the DPC formation corroborate results from the Gates and Wang laboratories showing the glutathionylation of β-elimination products of AP sites in nDNA (30,50). Additional studies are needed to clarify which type(s) of TFAM-induced DNA modifications are more persistent *in vivo*.

The accumulation of TFAM-DPCs in HeLa cells under limited GSH (∼70% relative to the control) and an elevated AP lesion level, but not the induction of AP sites alone, suggests a role of GSH in regulating the TFAM-DPC formation. Interestingly, in HEK293 cells, we observed that an elevation of mitochondrial AP site level is sufficient to cause a statistically significant increase of TFAM-DPCs (25). This can be explained by the overall lower level of total cellular glutathione (GSH and GSSG) in HEK293 cells compared to HeLa cells (51). The reaction of GSH with 3′pUA is consistent with the protective role of GSH against a variety of α,β-unsaturated carbonyl compounds from endogenous and exogenous sources (52,53). Considering that the level of GSH in mitochondria can fluctuate (35) and potentially less accessible to the interior of nucleoids, TFAM-DPCs and GSH-adducted SSB potentially co-exist *in vivo*, especially under conditions such as oxidative stress and exposure to toxic chemicals (52,53). Previously, a different type of mitochondrial DPC derived from a mutant form of tyrosyl-DNA phosphodiesterase 1 (TDP1) has been shown to form in human cells (54). The TDP1-DPC promotes mitochondrial dysfunction and mitophagy. Clearly, the formation and repair of TFAM-DPC under different cellular conditions warrant further investigation. Although proteolytic digestion has been shown to be a critical step in the repair of DPCs in the nucleus (2,4), whether mitochondrial DPCs would adopt similar strategies for repair or simply opt for degradation remains to be clarified.

The formation of TFAM-DPCs resembles the stable DPCs formed between AP sites and SRAP-domain proteins, albeit with different cross-linking chemistry. As a sensor of AP sites, HMCES forms DPCs to shield AP sites from error-prone processing in the nucleus (13,14). On the other hand, considering the multi-copy characteristic of mtDNA, protection of AP sites may not be as critical as with nuclear AP sites, in keeping with the rapid decline of mtDNA copy number and moderate accumulation of AP sites observed in the present study. Notably, a number of studies have shown that induction of AP sites (and other types of DNA lesions) leads to a decline in mtDNA copy number without increasing the mutation load of mtDNA in mammalian cell cultures (55) and animal models (56). Collectively, these observations support the importance of mtDNA turnover in processing mtDNA damage. TFAM-DPCs and GSH-adducted SSB may function as signals to recruit additional factors in mtDNA turnover or in the purifying selection of healthy mtDNA molecules (Figure 5). In addition, considering that AP sites likely encounter other mtDNA-binding proteins, the seemingly suicidal reaction with TFAM may shield AP sites from DPC formation with other less abundant but essential mtDNA enzymes, such as DNA polymerase γ (57).

In conclusion, the present study provides the first evidence for the formation of stable DPCs in cultured human cells between a major mtDNA-packaging protein, TFAM, and ubiquitous AP sites. Our compelling data from biochemical and cellular experiments demonstrate that TFAM processes AP sites efficiently and form TFAM-DPCs and SSB. The biochemical and cellular evidence in this study, along with the robust competition of TFAM with a DNA repair enzyme, AP endonuclease 1 reported earlier (23), argues strongly that TFAM is involved in AP-DNA turnover in mitochondria in cultured human cells.

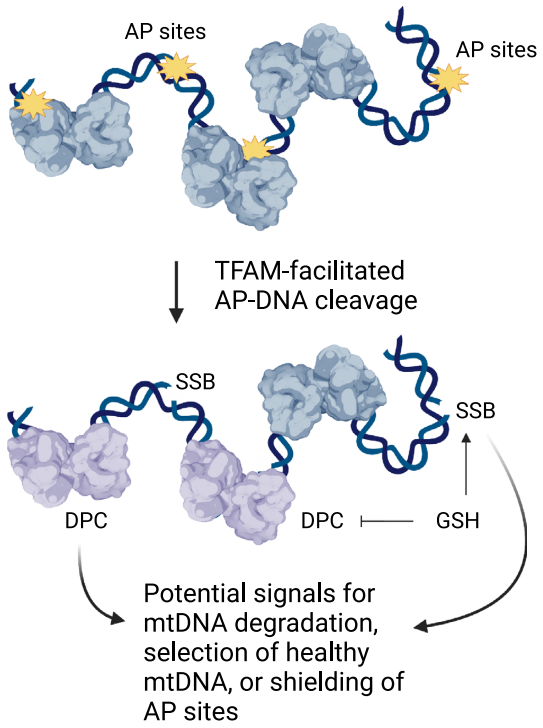

Figure 5. Formation of DPCs and SSB in TFAM-mediated AP-DNA cleavage and the proposed role of DPCs and SSB as potential signals for mtDNA degradation, purifying selection of mtDNA, or protection of AP sites from erroneous processing. Noncovalently associated TFAM molecules are in blue, and covalently linked TFAM molecules are in purple (created with BioRender.com).

DATA AVAILABILITY

The data underlying this article are available in the article and in its online supplementary material.

SUPPLEMENTARY DATA

Supplementary Data are available at NAR Online.

ACKNOWLEDGEMENTS

We thank Dr. Laurie S. Kaguni for critically reading the manuscript, Wenxin Zhao for contributing to the expression and purification of TFAM and TFAM C49S, and Dylan Tonthat for assistance with site-directed mutagenesis.

FUNDING

National Institutes of Health (NIH) [R35 GM128854 to L.Z.]; University of California, Riverside. Funding for open access charge: National Institutes of Health and University of California.
Conflict of interest statement. None declared.

REFERENCES

1. Stingele,J., Bellelli,R. and Boulton,S.J. (2017) Mechanisms of DNA–protein crosslink repair. *Nat. Rev. Mol. Cell Biol.*, **18**, 563–573.
2. Weickert,P. and Stingele,J. (2022) DNA–protein crosslinks and their resolution. *Annu. Rev. Biochem.*, **91**, 157–181.
3. Tretyakova,N.Y., Groehler,A. and Ji,S. (2015) DNA–protein cross-links: formation, structural identities, and biological outcomes. *Acc. Chem. Res.*, **48**, 1631–1644.
4. Wei,X., Peng,Y., Bryan,C. and Yang,K. (2021) Mechanisms of DNA− protein cross-link formation and repair. *Biochim. Biophys. Acta Proteins Proteomics*, **1869**, 140669.
5. Swenberg,J.A., Lu,K., Moeller,B.C., Gao,L.N., Upton,P.B., Nakamura,J. and Starr,T.B. (2011) Endogenous versus exogenous DNA adducts: their role in carcinogenesis, epidemiology, and risk assessment. *Toxicol. Sci.*, **120**, S130–S145.
6. Nakamura,J., Mutlu,E., Sharma,V., Collins,L., Bodnar,W., Yu,R., Lai,Y., Moeller,B., Lu,K. and Swenberg,J. (2014) The endogenous exposome. *DNA Repair (Amst.)*, **19**, 3–13.
7. Greenberg,M.M. (2014) Looking beneath the surface to determine what makes DNA damage deleterious. *Curr. Opin. Chem. Biol.*, **21**, 48–55.
8. Thompson,P.S. and Cortez,D. (2020) New insights into abasic site repair and tolerance. *DNA Repair (Amst.)*, **90**, 102866.
9. Nakamura,J. and Nakamura,M. (2020) DNA–protein crosslink formation by endogenous aldehydes and AP sites. *DNA Repair (Amst.)*, **88**, 102806.
10. Sczepanski,J.T., Wong,R.S., McKnight,J.N., Bowman,G.D. and Greenberg,M.M. (2010) Rapid DNA–protein cross-linking and strand scission by an abasic site in a nucleosome core particle. *Proc. Natl. Acad. Sci. U.S.A.*, **107**, 22475–22480.
11. Yang,K., Park,D., Tretyakova,N.Y. and Greenberg,M.M. (2018) Histone tails decrease N7-methyl-2′-deoxyguanosine depurination and yield DNA–protein cross-links in nucleosome core particles and cells. *Proc. Natl. Acad. Sci. U.S.A.*, **115**, E11212–E11220.
12. Thompson,P.S., Amidon,K.M., Mohni,K.N., Cortez,D. and Eichman,B.F. (2019) Protection of abasic sites during DNA replication by a stable thiazolidine protein-DNA cross-link. *Nat. Struct. Mol. Biol.*, **26**, 613–618.
13. Mohni,K.N., Wessel,S.R., Zhao,R., Wojciechowski,A.C., Luzwick,J.W., Layden,H., Eichman,B.F., Thompson,P.S., Mehta,K.P. and Cortez,D. (2019) HMCES maintains genome integrity by shielding abasic sites in single-strand DNA. *Cell*, **176**, 144–153.
14. Mehta,K.P.M., Lovejoy,C.A., Zhao,R., Heintzman,D.R. and Cortez,D. (2020) HMCES maintains replication fork progression and prevents double-strand breaks in response to APOBEC deamination and abasic site formation. *Cell Rep.*, **31**, 107705.
15. Semlow,D.R., MacKrell,V.A. and Walter,J.C. (2022) The HMCES DNA–protein cross-link functions as an intermediate in DNA interstrand cross-link repair. *Nat. Struct. Mol. Biol.*, **29**, 451–462.
16. Zhao,L. and Sumberaz,P. (2020) Mitochondrial DNA damage: prevalence, biological consequence, and emerging pathways. *Chem. Res. Toxicol.*, **33**, 2491–2502.
17. Gustafson,M.A., Sullivan,E.D. and Copeland,W.C. (2020) Consequences of compromised mitochondrial genome integrity. *DNA Repair (Amst.)*, **93**, 102916.
18. Gustafsson,C.M., Falkenberg,M. and Larsson,N.-G. (2016) Maintenance and expression of mammalian mitochondrial DNA. *Annu. Rev. Biochem.*, **85**, 133–160.
19. Alexeyev,M., Shokolenko,I., Wilson,G. and LeDoux,S. (2013) The maintenance of mitochondrial DNA integrity—critical analysis and update. *Cold Spring Harb. Perspect. Biol.*, **5**, a012641.
20. Craven,L., Alston,C.L., Taylor,R.W. and Turnbull,D.M. (2017) Recent advances in mitochondrial disease. *Annu. Rev. Genom. Hum. Genet.*, **18**, 257–275.
21. Trifunovic,A., Wredenberg,A., Falkenberg,M., Spelbrink,J.N., Rovio,A.T., Bruder,C.E., Bohlooly-Y,M., Gidlöf,S., Oldfors,A. and Wibom,R. (2004) Premature ageing in mice expressing defective mitochondrial DNA polymerase. *Nature*, **429**, 417–423.
22. Campbell,C.T., Kolesar,J.E. and Kaufman,B.A. (2012) Mitochondrial transcription factor A regulates mitochondrial transcription initiation, DNA packaging, and genome copy number. *Biochim. Biophys. Acta, Gene Regul. Mech.*, **1819**, 921–929.
23. Xu,W., Boyd,R.M., Tree,M.O., Samkari,F. and Zhao,L. (2019) Mitochondrial transcription factor A promotes DNA strand cleavage at abasic sites. *Proc. Natl. Acad. Sci. U.S.A.*, **116**, 17792–17799.
24. Tang,J., Zhao,W., Hendricks,N.G. and Zhao,L. (2021) High-Resolution Mapping of Amino Acid Residues in DNA–Protein Cross-Links Enabled by Ribonucleotide-Containing DNA. *Anal. Chem.*, **93**, 13398–13406.

25. Xu,W. and Zhao,L. (2022) An enzyme-linked immunosorbent assay for the detection of mitochondrial DNA–protein cross-links from mammalian cells. *DNA*, **2**, 264–278.
26. Ngo,H.B., Kaiser,J.T. and Chan,D.C. (2011) The mitochondrial transcription and packaging factor Tfam imposes a U-turn on mitochondrial DNA. *Nat. Struct. Mol. Biol.*, **18**, 1290–1296.
27. Rubio-Cosials,A., Sydow,J.F., Jiménez-Menéndez,N., Fernández-Millán,P., Montoya,J., Jacobs,H.T., Coll,M., Bernadó,P. and Solà,M. (2011) Human mitochondrial transcription factor A induces a U-turn structure in the light strand promoter. *Nat. Struct. Mol. Biol.*, **18**, 1281–1289.
28. Housh,K., Jha,J.S., Yang,Z., Haldar,T., Johnson,K.M., Yin,J., Wang,Y. and Gates,K.S. (2021) Formation and repair of an interstrand DNA cross-link arising from a common endogenous lesion. *J. Am. Chem. Soc.*, **143**, 15344–15357.
29. Bailly,V. and Verly,W.G. (1987) Escherichia coli endonuclease III is not an endonuclease but a β-elimination catalyst. *Biochem. J.*, **242**, 565–572.
30. Jha,J.S., Yin,J., Haldar,T., Wang,Y. and Gates,K.S. (2022) Reconsidering the Chemical Nature of Strand Breaks Derived from Abasic Sites in Cellular DNA: evidence for 3′-Glutathionylation. *J. Am. Chem. Soc.*, **144**, 10471–10482.
31. Müller,T.A., Tobar,M.A., Perian,M.N. and Hausinger,R.P. (2017) Biochemical characterization of AP lyase and m6A demethylase activities of human AlkB homologue 1 (ALKBH1). *Biochemistry*, **56**, 1899–1910.
32. Levin,J.D., Johnson,A.W. and Demple,B. (1988) Homogeneous *Escherichia coli* endonuclease IV. Characterization of an enzyme that recognizes oxidative damage in DNA. *J. Biol. Chem.*, **263**, 8066–8071.
33. D'Ham,C., Romieu,A., Jaquinod,M., Gasparutto,D. and Cadet,J. (1999) Excision of 5, 6-dihydroxy-5, 6-dihydrothymine, 5, 6-dihydrothymine, and 5-hydroxycytosine from defined sequence oligonucleotides by *Escherichia coli endonuclease* III and Fpg proteins: kinetic and mechanistic aspects. *Biochemistry*, **38**, 3335–3344.
34. Darwanto,A., Farrel,A., Rogstad,D.K. and Sowers,L.C. (2009) Characterization of DNA glycosylase activity by matrix-assisted laser desorption/ionization time-of-flight mass spectrometry. *Anal. Biochem.*, **394**, 13–23.
35. Marí,M., Morales,A., Colell,A., García-Ruiz,C. and Fernández-Checa,J.C. (2009) Mitochondrial glutathione, a key survival antioxidant. *Antioxid. Redox Signal.*, **11**, 2685–2700.
36. Rubio-Cosials,A., Battistini,F., Gansen,A., Cuppari,A., Bernadó,P., Orozco,M., Langowski,J., Tóth,K. and Solà,M. (2018) Protein flexibility and synergy of HMG domains underlie U-turn bending of DNA by TFAM in solution. *Biophys. J.*, **114**, 2386–2396.
37. Cuppari,A., Fernández-Millán,P., Battistini,F., Tarrés-Solé,A., Lyonnais,S., Iruela,G., Ruiz-Lopez,E., Enciso,Y., Rubio-Cosials,A. and Prohens,R. (2019) DNA specificities modulate the binding of human transcription factor A to mitochondrial DNA control region. *Nucleic Acids Res.*, **47**, 6519–6537.
38. Choi,W.S. and Garcia-Diaz,M. (2022) A minimal motif for sequence recognition by mitochondrial transcription factor A (TFAM). *Nucleic Acids Res.*, **50**, 322–332.
39. Shokolenko,I.N., Wilson,G.L. and Alexeyev,M.F. (2013) Persistent damage induces mitochondrial DNA degradation. *DNA Repair (Amst.)*, **12**, 488–499.
40. Kavli,B., Slupphaug,G., Mol,C.D., Arvai,A.S., Peterson,S.B., Tainer,J.A. and Krokan,H.E. (1996) Excision of cytosine and thymine from DNA by mutants of human uracil-DNA glycosylase. *EMBO J.*, **15**, 3442.
41. Qian,W., Kumar,N., Roginskaya,V., Fouquerel,E., Opresko,P.L., Shiva,S., Watkins,S.C., Kolodieznyi,D., Bruchez,M.P. and Van Houten,B. (2019) Chemoptogenetic damage to mitochondria causes rapid telomere dysfunction. *Proc. Natl. Acad. Sci. U.S.A.*, **116**, 18435–18444.
42. Nadalutti,C.A., Ayala-Peña,S. and Santos,J.H. (2022) Mitochondrial DNA damage as driver of cellular outcomes. *Am. J. Physiol. Cell Physiol.*, **322**, C136–C150.
43. Drew,R. and Miners,J.O. (1984) The effects of buthionine sulphoximine (BSO) on glutathione depletion and xenobiotic biotransformation. *Biochem. Pharmacol.*, **33**, 2989–2994.
44. Shokolenko,I.N. and Alexeyev,M.F. (2015) Mitochondrial DNA: a disposable genome?*Biochim. Biophys. Acta, Mol. Basis Dis.*, **1852**, 1805–1809.
45. Matic,S., Jiang,M., Nicholls,T.J., Uhler,J.P., Dirksen-Schwanenland,C., Polosa,P.L., Simard,M.-L., Li,X., Atanassov,I. and Rackham,O. (2018) Mice lacking the mitochondrial exonuclease MGME1 accumulate mtDNA deletions without developing progeria. *Nat. Commun.*, **9**, 1202.
46. Nissanka,N., Bacman,S.R., Plastini,M.J. and Moraes,C.T. (2018) The mitochondrial DNA polymerase gamma degrades linear DNA fragments precluding the formation of deletions. *Nat. Commun.*, **9**, 2491.
47. Peeva,V., Blei,D., Trombly,G., Corsi,S., Szukszto,M.J., Rebelo-Guiomar,P., Gammage,P.A., Kudin,A.P., Becker,C. and Altmüller,J. (2018) Linear mitochondrial DNA is rapidly degraded by components of the replication machinery. *Nat. Commun.*, **9**, 1727.
48. Xian,H., Watari,K., Sanchez-Lopez,E., Offenberger,J., Onyuru,J., Sampath,H., Ying,W., Hoffman,H.M., Shadel,G.S. and Karin,M. (2022) Oxidized DNA fragments exit mitochondria via mPTP-and VDAC-dependent channels to activate NLRP3 inflammasome and interferon signaling. *Immunity*, **55**, 1370–1385.
49. Wei,X., Wang,Z., Hinson,C. and Yang,K. (2022) Human TDP1, APE1 and TREX1 repair 3′-DNA–peptide/protein cross-links arising from abasic sites in vitro. *Nucleic Acids Res.*, **50**, 3638–3657.
50. Yin,J., Gates,K.S. and Wang,Y. (2022) N-methyl-N-nitrosourea induced 3′-glutathionylated DNA-cleavage products in mammalian cells. *Anal. Chem.*, **94**, 15595–15603.
51. Hansen,R.E., Roth,D. and Winther,J.R. (2009) Quantifying the global cellular thiol–disulfide status. *Proc. Natl. Acad. Sci. U.S.A.*, **106**, 422–427.
52. Janzowski,C., Glaab,V., Mueller,C., Straesser,U., Kamp,H. and Eisenbrand,G. (2003) α, β-Unsaturated carbonyl compounds: induction of oxidative DNA damage in mammalian cells. *Mutagenesis*, **18**, 465–470.
53. Kumagai,Y. and Abiko,Y. (2017) Environmental electrophiles: protein adducts, modulation of redox signaling, and interaction with persulfides/polysulfides. *Chem. Res. Toxicol.*, **30**, 203–219.
54. Ghosh,A., Bhattacharjee,S., Chowdhuri,S.P., Mallick,A., Rehman,I., Basu,S. and Das,B.B. (2019) SCAN1-TDP1 trapping on mitochondrial DNA promotes mitochondrial dysfunction and mitophagy. *Sci. Adv.*, **5**, eaax9778.
55. Kozhukhar,N., Spadafora,D., Fayzulin,R., Shokolenko,I.N. and Alexeyev,M. (2016) The efficiency of the translesion synthesis across abasic sites by mitochondrial DNA polymerase is low in mitochondria of 3T3 cells. *Mitochondrial DNA Part A*, **27**, 4390–4396.
56. Lauritzen,K.H., Moldestad,O., Eide,L., Carlsen,H., Nesse,G., Storm,J.F., Mansuy,I.M., Bergersen,L.H. and Klungland,A. (2010) Mitochondrial DNA toxicity in forebrain neurons causes apoptosis, neurodegeneration, and impaired behavior. *Mol. Cell. Biol.*, **30**, 1357–1367.
57. Longley,M.J., Prasad,R., Srivastava,D.K., Wilson,S.H. and Copeland,W.C. (1998) Identification of 5′-deoxyribose phosphate lyase activity in human DNA polymerase γ and its role in mitochondrial base excision repair in vitro. *Proc. Natl. Acad. Sci. U.S.A.*, **95**, 12244–12248.